Implementation of Unscented Kalman Filter and Complementary Filter applied to the ASSE scheme for Synthetic Flow Angles Estimation

Implementation of Unscented Kalman Filter and Complementary Filter applied to the ASSE scheme for Synthetic Flow Angles Estimation

Luca de Pasquale*, Gabriele Tarascio†, Angelo Lerro‡ and Piero Gili§
Department of Mechanical and Aerospace Engineering, Polytechnic University of Turin
Turin, Italy
Email: *luca.depasquale@polito.it, †gabriele.tarascio@polito.it, ‡angelo.lerro@polito.it, §piero.gili@polito.it

***Abstract*—This paper presents the results of the implementation of a quaternion-based Unscented Kalman Filter (UKF) and a Complementary Filter (CF), for attitude estimation, along with the Angle of Attack and Sideslip Estimator technology (ASSE), in order to provide an Air Data Synthetic Sensor for aerodynamic angles estimation. The attitude estimation is crucial for the computation of the full rotation matrix from the Inertial Reference Frame to the Body Reference Frame, needed by the ASSE algorithm. The estimation at issue exploits an Inertial Measurement Unit (IMU) equipped with a three-axis accelerometer, a gyroscope, a magnetometer and a Global Positioning System (GPS) receiver. Firstly, the filter algorithm is implemented in MATLAB and Simulink environment and its performance is assessed by using the measurements of a Flight Test Instrumentation (FTI) unit, a technological demonstrator built in Polytechnic University of Turin which encompasses the IMU. The verification is carried out with a series of tests employing a motion table at the National Metrology Institute of Italy (INRiM). Finally, the implementation of the filter with the ASSE technology is successfully demonstrated through a set of flight simulation data.**

***Index Terms*—Synthetic Sensors, Nonlinear Kalman filter, Complementary filter, Air Data, Quaternion, Flight Test Instrumention**

I. Introduction

Avionic systems are becoming significantly more complex in recent years, due to the increased demand for autonomous platforms, such as Unmanned Aircraft Vehicles (UAVs). This has led on to increasingly more stringent requirements on the accuracy and reliability of onboard avionic systems, particularly those related to navigation [10]. At the same time, advancements in the field of synthetic sensors have allowed to achieve increasingly reliable and accurate algorithms to indirectly measure quantities of interest. In particular, the use of synthetic sensors for air data estimation plays a key role in the improvement of flight safety, since it provides redundancy as well as additional failure detection capabilities, without the drawback of having additional hardware on board.

In this framework, the implementation of an Unscented Kalman Filter (UKF) with a Complementary Filter (CF) and the Angle of Attack and Sideslip Estimator technology (ASSE) is proposed, in order to develop a Synthetic Sensor (SS) for the aerodynamic angle estimation.

Air Data synthetic sensors allow to replace physical sensors, with benefits in terms of weight, maintainability, reliability, power consumption and emissions. A synthetic aerodynamic angles estimator called ASSE has been developed and patented at Polytechnic University of Turin, and it is thoroughly presented in [1]. As reported by Lerro et al., ASSE is a model-free scheme, developed to compute aerodynamic angles, that does not need an aircraft model or a flight test database. This aspect makes the scheme independent from the aircraft configuration and the flight regime, that instead strongly affect model-based and data-driven synthetic sensors. A key aspect of the ASSE algorithm is that it requires a precise attitude estimation, so as to compute and consider the appropriate change in external wind and the acceleration in the Body Reference Frame. This is the reason why the integration of this technology along with UKF and CF is taken into account.

The UKF was proposed for the first time in [2] by Julier and Uhlman, as a new extension of the Kalman Filter for nonlinear systems, demonstrating its ability, through a set of discretely sampled points used to parametrise mean and covariance, to perform equally to the KF in linear systems and better than the Extended Kalman Filter (EKF) in nonlinear systems, without the linearisation steps required. Indeed, for highly nonlinear systems, the state distribution, approximated by a Gaussian Random Variable (GRV) is propagated analytically through the first order linearization of the system. This can introduce very large errors in the true posterior mean and covariance of the transformed GRV, that may lead to sub-optimal performance and divergence of the filter.

Thanks to the Unscented Transformation, explained in the following section, the UKF could achieve greater attitude estimation performance than the EKF, as demonstrated in several previous studies [3]– [6]. In detail, [3] and [5] proved the success of the UKF for spacecraft attitude estimation, while [4] discussed the great capability of the UKF to deal with large and small attitude errors of an inertial navigation system. In [6], the authors reported a UKF design for the attitude estimation of a strapdown inertial navigation system. In [8], the authors present an integration of the UKF with a CF.

This paper is structured as follows. Section II describes the ASSE scheme, for aerodynamic angles estimation, and the UKF and CF algorithm, for the attitude estimation. A description of the FTI setup is also provided in this section.

The details of the tests conducted, along with the results obtained, are discussed in Section III. Finally, Section IV draws the conclusions for the present work.

II. Method

A. ASSE algorithm

The final system of the ASSE algorithm is derived from an initial rearrangement of flight mechanic equations. In particular, starting from the inertial acceleration, projected on the Body Reference Frame (BRF), it is possible to write the following equation:

$$\boldsymbol{a}_B = C_{I2B}\mathbf{a}_I = \dot{\boldsymbol{v}}_B + \boldsymbol{\Omega}_B\,\boldsymbol{v}_B + C_{I2B}\dot{\boldsymbol{w}} \tag{1}$$

where: $\boldsymbol{a}_B$ is the inertial acceleration measured on board, expressed in BRF; $\boldsymbol{v}_B$ is aircraft velocity in BRF; $\boldsymbol{\Omega}_B$ is the skew-symmetric matrix obtained from the angular velocity in BRF ($\boldsymbol{\omega}_B = [p, q, r]^T$) as:

$$\boldsymbol{\Omega}_B = \begin{bmatrix} 0 & -r & q \\ r & 0 & -p \\ -q & p & 0 \end{bmatrix} \tag{2}$$

Moreover, C_{I2B} is the full rotation matrix from the Inertial Reference Frame (IRF) to the BRF, given by:

$$C_{I2B} = \begin{bmatrix} C_\theta C_\psi & C_\theta S_\psi & -S_\theta \\ S_\varphi S_\theta C_\psi - C_\varphi S_\psi & S_\varphi S_\theta S_\psi + C_\varphi C_\psi & S_\varphi C_\theta \\ C_\varphi S_\theta C_\psi + S_\varphi S_\psi & C_\varphi S_\theta S_\psi - S_\varphi C_\psi & C_\varphi C_\theta \end{bmatrix} \tag{3}$$

where ψ, θ and φ are the three Euler angles, hereby referred to as yaw, pitch and roll, respectively. Here and throughout the paper, the following conventions are adopted for ease of notation: $C_\xi \equiv \cos\xi$ and $S_\xi \equiv \sin\xi$, where ξ is a generic angle. Finally, $\dot{\boldsymbol{w}}$ is the time derivative of the wind velocity, expressed in IRF.

From (1), it is possible to write the acceleration $\dot{\boldsymbol{v}}_B$ as:

$$\dot{\boldsymbol{v}}_B = \boldsymbol{a}_B - \boldsymbol{\Omega}_B\boldsymbol{v}_B - C_{I2B}\dot{\boldsymbol{w}} \tag{4}$$

Remembering that:

$$\dot{V}_\infty = \frac{\boldsymbol{v}_B^T\dot{\boldsymbol{v}}_B}{V_\infty} + \boldsymbol{w} \tag{5}$$

where V_∞ is the true airspeed (TAS) of the aircraft, and substituting $\dot{\boldsymbol{v}}_B$ with its expression in (4), the following equation is obtained:

$$\dot{V}_\infty V_\infty = \boldsymbol{v}_B^T\dot{\boldsymbol{v}}_B = \boldsymbol{v}_B^T(\boldsymbol{a}_B - C_{I2B}\dot{\boldsymbol{w}}) \tag{6}$$

where all terms refer to the same time instant.

Considering the hypothesis that the relative velocity vector $\boldsymbol{v}_B$ in (5), and so the aerodynamic angles, at a certain time instant t can be modelled using information from the past, starting from $\boldsymbol{v}_B$ at a generic time instant τ, with $t \geq \tau$, $\boldsymbol{v}_{B,t}$ can be expressed as

$$\boldsymbol{v}_{B,t} = \boldsymbol{v}_{B,\tau} + \int_\tau^t \dot{\boldsymbol{v}}_B(T)\,dT \tag{7}$$

Recalling (4), equation (7) can be written as

$$\boldsymbol{v}_{B,t} = \boldsymbol{v}_{B,\tau} + \int_\tau^t (\boldsymbol{a}_B - \boldsymbol{\Omega}_B\boldsymbol{v}_B - C_{I2B}\dot{\boldsymbol{w}})\,dT \tag{8}$$

and

$$\boldsymbol{v}_{B,\tau} = \boldsymbol{v}_{B,t} - \int_\tau^t \boldsymbol{a}_B\,dT + \int_\tau^t \boldsymbol{\Omega}_B\,\boldsymbol{v}_B\,dT + \int_\tau^t C_{I2B}\dot{\boldsymbol{w}}\,dT \tag{9}$$

Replacing $\boldsymbol{v}_{B,\tau}$ with (9), equation (5) can be written at time τ as

$$\begin{aligned} \dot{V}_{\infty,\tau}V_{\infty,\tau} = &\left[\boldsymbol{v}_{B,t} - \int_\tau^t \boldsymbol{a}_B\,dT + \right. \\ &\left. \int_\tau^t \boldsymbol{\Omega}_B\,\boldsymbol{v}_B\,dT + \int_\tau^t C_{I2B}\dot{\boldsymbol{w}}\,dT\right]^T (\boldsymbol{a}_B - C_{I2B}\dot{\boldsymbol{w}})_\tau \\ &\implies \dot{V}_{\infty,\tau}V_{\infty,\tau} + \\ &\left[\int_\tau^t \boldsymbol{a}_B\,dT - \int_\tau^t C_{I2B}\dot{\boldsymbol{w}}\,dT\right]^T (\boldsymbol{a}_B - C_{I2B}\dot{\boldsymbol{w}})_\tau = \\ &\left[\boldsymbol{v}_{B,t} + \int_\tau^t \boldsymbol{\Omega}_B\,\boldsymbol{v}_B\,dT\right]^T (\boldsymbol{a}_B - C_{I2B}\dot{\boldsymbol{w}})_\tau \end{aligned} \tag{10}$$

where all terms which depend on $\boldsymbol{v}_B$, and hence aerodynamic angles, are collected on the right-hand side.

Furthermore, recalling matrix properties and considering the assumption that the integrand function is constant in the generic time interval $[\tau, t]$ ("zero-order approximation" hypothesis, detailed in [9]), equation (10) can be written as

$$\begin{aligned} &\dot{V}_{\infty,\tau}V_{\infty,\tau} + \\ &\left[\int_\tau^t \boldsymbol{a}_B\,dT - \int_\tau^t C_{I2B}\dot{\boldsymbol{w}}\,dT\right]^T (\boldsymbol{a}_B - C_{I2B}\dot{\boldsymbol{w}})_\tau \\ &= V_{\infty,\tau}\hat{\boldsymbol{i}}_{WB,t}^T\,(\boldsymbol{I} - \boldsymbol{\Omega}_{B,t}\Delta t)\,(\boldsymbol{a}_B - C_{I2B}\dot{\boldsymbol{w}})_\tau \end{aligned} \tag{11}$$

where

$$\boldsymbol{v}_B = V_\infty\hat{\boldsymbol{i}}_{WB,t}^T \tag{12}$$

and, denoting the angle of attack and the angle of side-slip with α and β respectively, the unit vector of the relative velocity in BRF $\hat{\boldsymbol{i}}_{WB,t}^T$ is written as:

$$\hat{\boldsymbol{i}}_{WB,t}^T = (C_\beta C_\alpha)\hat{\boldsymbol{i}}_B + S_\beta\hat{\boldsymbol{j}}_B + (C_\beta S_\alpha)\hat{\boldsymbol{k}}_B \tag{13}$$

where $\hat{\boldsymbol{i}}_B$, $\hat{\boldsymbol{j}}_B$ and $\hat{\boldsymbol{k}}_B$ denote the unit vectors of the BRF axes.

Equation (11) is the basic expression of the zero-order ASSE scheme, referred to the generic time τ where the aerodynamic angles $\alpha(t)$ and $\beta(t)$ are the only unknowns. All other terms are measured.

Hence, the aerodynamic angles estimation proposed in the ASSE algorithm is based on direct measurement of the true airspeed, V_∞, its time derivative, $\dot{V}_\infty$, the inertial body acceleration, $\boldsymbol{a}_B$, angular rates and the wind field.

To simplify the notation, the measurable quantities of (11) are grouped and denoted as:

$$\begin{aligned} n_\tau = &\dot{V}_{\infty,\tau}V_{\infty,\tau} + \\ &\left[\int_\tau^t \boldsymbol{a}_B\,dT - \int_\tau^t C_{I2B}\dot{\boldsymbol{w}}\,dT\right]^T (\boldsymbol{a}_B - C_{I2B}\dot{\boldsymbol{w}})_\tau \end{aligned} \tag{14}$$

whilst the right-hand side is denoted as:

$$\begin{aligned}\boldsymbol{m}_\tau = V_{\infty,\tau}\hat{\boldsymbol{i}}_{WB,t}^T\left(\boldsymbol{I}-\boldsymbol{\Omega}_{B,t}\Delta t\right)\left(\boldsymbol{a}_B - C_{I2B}\dot{\boldsymbol{w}}\right)_\tau \\ = h_\tau\hat{\boldsymbol{i}}_B + l_\tau\hat{\boldsymbol{j}}_B + m_\tau\hat{\boldsymbol{k}}_B\end{aligned} \quad (15)$$

Therefore, writing (11) in a more compact form and expanding back in time starting from t to the n-th generic τ_i with $i=[0,1,\ldots,n]$, where $\tau_0=t$, a system of $n+1$ nonlinear equations is obtained:

$$\begin{cases} n_t = \boldsymbol{m}_t\hat{\boldsymbol{i}}_{WB,t}^T = h_tC_\beta C_\alpha + l_tS_\beta + m_tC_\beta S_\alpha \\ n_{\tau_1} = \boldsymbol{m}_{\tau_1}\hat{\boldsymbol{i}}_{WB,t}^T = h_{\tau_1}C_\beta C_\alpha + l_{\tau_1}S_\beta + m_{\tau_1}C_\beta S_\alpha \\ \vdots \\ n_{\tau_n} = \boldsymbol{m}_{\tau_n}\hat{\boldsymbol{i}}_{WB,t}^T = h_{\tau_n}C_\beta C_\alpha + l_{\tau_n}S_\beta + m_{\tau_n}C_\beta S_\alpha \end{cases} \quad (16)$$

Equation (16) is the generic form of the zero-order ASSE scheme, based on $n+1$ equations.

To the previous equations, an additional one is considered which corresponds to the constraint that $\hat{\boldsymbol{i}}_{WB,t}$ is a unit vector, therefore:

$$\hat{\boldsymbol{i}}_{WB,t}^T\hat{\boldsymbol{i}}_{WB,t} = 1 \quad (17)$$

Adding this condition and writing (16) in a more compact matrix form by using the notations $\boldsymbol{n}_n = [n_t, n_{\tau_1},\ldots,n_{\tau_n}]$ and $\boldsymbol{M}_n = \left[\boldsymbol{m}_t^T,\boldsymbol{m}_{\tau_1}^T,\ldots,\boldsymbol{m}_{\tau_n}^T\right]^T$, the nonlinear system of equations based on the zero-order ASSE scheme is obtained:

$$\begin{cases} 1 = \hat{\boldsymbol{i}}_{WB,t}^T\hat{\boldsymbol{i}}_{WB,t} \\ \boldsymbol{n}_n = \boldsymbol{M}_n\hat{\boldsymbol{i}}_{WB,t} \end{cases} \quad (18)$$

B. UKF and CF algorithms

The UKF addresses the problem of the reduction in performance that can be seen when applying a first-order linearization to a non-linear system. Such performance decrease usually depends on how well the non-linear system is approximated by the linear one. The UKF solves this issue by using a deterministic sampling approach instead of linearizing.

As in the EKF, the state distribution is approximated by a GRV, but it is now represented using a minimal set of carefully chosen sample points, which completely capture the true mean and covariance of the GRV and, when propagated through the true nonlinear system, capture the posterior mean and covariance accurately to the third order of the Taylor series expansion for any nonlinearity. Additionally, the computational complexity of the UKF maintains the same order as that of the EKF.

The Unscented Transformation (UT), on which the UKF is based, is a method for calculating the statistics of a random variable which undergoes a nonlinear transformation. Consider the propagation of a random variable $\boldsymbol{x}$, with dimension L, through a nonlinear function $\boldsymbol{y}=g(\boldsymbol{x})$ and assume that $\boldsymbol{x}$ has mean $\bar{\boldsymbol{x}}$ and covariance $\boldsymbol{P}_{\boldsymbol{x}}$. To calculate the statistics of $\boldsymbol{y}$ we form a matrix $\boldsymbol{\chi}$ of $2L+1$ sigma vectors χ_i, with corresponding weights W_i:

$$\begin{aligned} \chi_0 &= \bar{\boldsymbol{x}} \\ \chi_i &= \bar{\boldsymbol{x}} + \left(\sqrt{(L+\lambda)\boldsymbol{P}_{\boldsymbol{x}}}\right)_i, \quad i=1,\ldots,L \\ \chi_i &= \bar{\boldsymbol{x}} - \left(\sqrt{(L+\lambda)\boldsymbol{P}_{\boldsymbol{x}}}\right)_i, \quad i=L+1,\ldots,2L \\ W_{m,0} &= \frac{\lambda}{L+\lambda} \\ W_{c,0} &= \frac{\lambda}{L+\lambda} + \left(1-\alpha^2+\beta\right) \\ W_{m,i} &= W_{c,i} = \frac{1}{2\left(L+\lambda\right)}, \quad i=1,\ldots,2L \end{aligned} \quad (19)$$

where $\lambda=\alpha^2\left(L+\kappa\right)-L$ is a scaling parameter, composed by α and κ; the former determines the spread of the sigma points around $\bar{\boldsymbol{x}}$ and assumes small positive values, whereas the latter is a secondary scaling parameter, usually set to 0. The parameter β, instead, takes into account the prior knowledge of the distribution of $\boldsymbol{x}$ and, for Gaussian distributions assumes the optimal value of 2 [7]. The term $\left(\sqrt{(L+\lambda)\boldsymbol{P}_{\boldsymbol{x}}}\right)_i$ is the i-th row of the matrix square root.

These sigma points are propagated through the nonlinear function:

$$\mathcal{Y}_i = g\left(\chi_i\right), \quad i=0,1,\ldots,2L \quad (20)$$

and the mean and covariance for $\boldsymbol{y}$ are approximated using the weighted sample mean and covariance of the posterior sigma points:

$$\begin{aligned} \bar{\boldsymbol{y}} &\approx \sum_{i=0}^{2L} W_{m,i}\mathcal{Y}_i \\ \boldsymbol{P}_{\boldsymbol{y}} &\approx \sum_{i=0}^{2L} W_{c,i}\left(\mathcal{Y}_i-\bar{\boldsymbol{y}}\right)\left(\mathcal{Y}_i-\bar{\boldsymbol{y}}\right)^T \end{aligned} \quad (21)$$

The UKF implemented in this work uses the pitch and roll angles, computed from gravity force decomposition, as the measurements for the filter. The four components of the quaternion are constrained, since, by definition, the magnitude of a quaternion must be one. This constraint is implemented in the filter as an additional measurement equation, treated as a perfect measurement and integrated into the filter computation.

The system model equations are:

$$\begin{cases} \boldsymbol{x}_{k+1} = f\left(\boldsymbol{x}_k,\boldsymbol{u}_k\right) + \boldsymbol{w}_k \\ \boldsymbol{y}_k = h\left(\boldsymbol{x}_k\right) + \boldsymbol{n}_k \end{cases} \quad (22)$$

where $\boldsymbol{x}$ represents the state vector, consisting of the quaternion components, $\boldsymbol{u}$ is the state input, the angular rate, $\boldsymbol{y}$ is the measurement vector, made of four components: the first three are the gravity vector components, while the fourth is equal to 1, as per the quaternion condition. $\boldsymbol{w}_k \sim \mathcal{N}(0,\boldsymbol{Q}_k)$ and $\boldsymbol{n}_k \sim \mathcal{N}(0,\boldsymbol{R}_k)$ are respectively the process noise and the measurement noise, both assumed to be zero-mean and Gaussian.

Since the state vector coincides with the attitude quaternion, the state update equation is given by:

$$\boldsymbol{q}_{k+1} = \left(I + \frac{\Delta t}{2} \boldsymbol{\Omega} \right) \boldsymbol{q}_k \tag{23}$$

where I is the 4×4 identity matrix, Δt is the simulation time step, q_k is the quaternion at time k and $\boldsymbol{\Omega}$, computed from the angular rate components, is given by:

$$\boldsymbol{\Omega} = \begin{bmatrix} 0 & -p & -q & -r \\ p & 0 & r & -q \\ q & -r & 0 & p \\ r & q & -p & 0 \end{bmatrix} \tag{24}$$

Hence, the state equation is:

$$f(x) = \left(I + \frac{\Delta t}{2} \boldsymbol{\Omega} \right) x \tag{25}$$

The measurement vector is given by:

$$\boldsymbol{z} = \begin{Bmatrix} \varphi_m \\ \theta_m \\ 1 \end{Bmatrix} \tag{26}$$

where φ_m is the measured roll angle and θ_m is the measured pitch angle. They are obtained from the measured gravity vector as follows:

$$\begin{aligned} \varphi_m &= \tan^{-1} \frac{g_y}{g_z} \\ \theta_m &= \tan^{-1} \frac{-g_x \cos \varphi_m}{g_z} \end{aligned} \tag{27}$$

From Euler angles and quaternion definitions:

$$\begin{Bmatrix} \varphi \\ \theta \\ \psi \end{Bmatrix} = \begin{Bmatrix} \tan^{-1} \frac{2(q_0 q_1 + q_2 q_3)}{q_0^2 - q_1^2 - q_2^2 + q_3^2} \\ \sin^{-1} 2(q_0 q_3 - q_1 q_2) \\ \tan^{-1} \frac{2(q_0 q_3 + q_1 q_2)}{q_0^2 + q_1^2 - q_2^2 + q_3^2} \end{Bmatrix} \tag{28}$$

From accelerometers and GPS measurements, it is possible to determine the gravity vector. Indicating the acceleration measured by the accelerometer as $\boldsymbol{a}_B$, the NED velocity and its derivative measured by the GPS as, respectively, $\boldsymbol{v}_{NED}$ and $\dot{\boldsymbol{v}}_{NED}$, the indirectly measured gravity vector is computed as:

$$\boldsymbol{g} = \boldsymbol{a}_B + \dot{\boldsymbol{v}}_B + \boldsymbol{\omega} \times \boldsymbol{v}_B \tag{29}$$

In (29), $\boldsymbol{\omega}$ is the angular rate and $\boldsymbol{v}_B$ and $\dot{\boldsymbol{v}}_B$ are, respectively, the body velocity and its derivative:

$$\begin{aligned} \boldsymbol{v}_B &= R_N^B \boldsymbol{v}_{NED} \\ \dot{\boldsymbol{v}}_B &= R_N^B \left\{ \dot{\boldsymbol{v}}_{NED} - \left[\left(R_N^B \right)^T \boldsymbol{\omega} \right] \times \boldsymbol{v}_{NED} \right\} \end{aligned} \tag{30}$$

where R_N^B is the rotation matrix from NED reference frame to BRF. The perfect measurement of the quaternion vector components is simply expressed by:

$$1 = \ q_0^2 + q_1^2 + q_2^2 + q_3^2 \tag{31}$$

Therefore, by combining (28) and (31), the measurement equation, $h(x)$, is given by:

$$h(x) = \begin{Bmatrix} \tan^{-1} \frac{2(x_1 x_2 + x_3 x_4)}{x_1^2 - x_2^2 - x_3^2 + x_4^2} \\ \sin^{-1} 2(x_1 x_3 - x_1 x_4) \\ x_1^2 + x_2^2 + x_3^2 + x_4^2 \end{Bmatrix} \tag{32}$$

The noise matrices Q_k and R_k are not constant and are computed as:

$$Q_k = L_k \widetilde{Q} L_k^T \tag{33}$$

$$R_k = M_{\varphi\theta} M_{xyz} R_{\varphi\theta} M_{xyz}^T M_{\varphi\theta}^T \tag{34}$$

where:

$$L_k = \frac{1}{2} \begin{bmatrix} -q_1 & -q_2 & -q_3 \\ q_0 & -q_3 & q_2 \\ q_3 & q_0 & -q_1 \\ -q_2 & q_1 & q_0 \end{bmatrix} \tag{35}$$

$$M_{\varphi\theta} = \begin{bmatrix} 0 & \frac{g_z}{g_y^2 + g_z^2} & -\frac{g_y}{g_y^2 + g_z^2} \\ \frac{-g_z C_\varphi}{g_x^2 C\varphi^2 + g_z^2} & \frac{g_x g_z^2 S_\varphi}{(g_y^2 + g_z^2)(g_x^2 C_\varphi^2 + g_z)} & \frac{(g_y^2 + g_z^2) g_x C_\varphi - g_x g_y g_z S_\varphi}{(g_y^2 + g_z^2)(g_x^2 C_\varphi^2 + g_z^2)} \end{bmatrix} \tag{36}$$

$$M_{xyz} = \begin{bmatrix} & 0 & r & -q & 0 & -w & v \\ [I]_{3\times3} & -r & 0 & p & w & 0 & -u \\ & q & -p & 0 & -v & u & 0 \end{bmatrix} \tag{37}$$

and the constant matrices $\widetilde{Q}$ and $R_{\varphi\theta}$ depend on the variances of the measured quantities (where σ_γ^2 indicates the variance of the generic quantity γ):

$$\widetilde{Q} = \text{diag}([\sigma_p^2, \sigma_q^2 \sigma_r^2]) \tag{38}$$

$$R_{\varphi\theta} = \text{diag}([\sigma_{a_x}^2, \sigma_{a_y}^2, \sigma_{a_z}^2, \sigma_u^2, \sigma_v^2, \sigma_w^2, \sigma_u^2, \sigma_v^2, \sigma_w^2, \sigma_p^2, \sigma_q^2 \sigma_r^2]) \tag{39}$$

The heading angle is obtained from a CF, which uses the heading signal derived from the magnetometer (ψ_m) and the GPS-derived heading (ψ_{GPS}) given by:

$$\psi_{GPS} = \tan^{-1} \left(\frac{v_E}{v_N} \right) \tag{40}$$

This fusion permits to achieve a long-term accurate, reliable and less noisy heading information. In particular, the CF is implemented with the equation:

$$\psi = \frac{2\zeta\omega_0 s + \omega_0^2}{s^2 + 2\zeta\omega_0 s + \omega_0^2} \psi_m + \frac{s^2}{s^2 + 2\zeta\omega_0 s + \omega_0^2} \psi_{GPS} \tag{41}$$

where ζ is the damping ratio of the filter and ω_0 is the natural frequency.

C. FTI setup

The scheme presented above has been implemented on a technological demonstrator, assembled in Polytechnic University of Turin, consisting of an FTI unit which encompasses a number of sensors to provide direct measurements to ASSE and the attitude estimator. In particular, as shown in Fig. 1 and Fig. 2, the unit includes:

- MEMS IMU: STIM318 by Sensonor;
- FOG gyroscope: DSP-1760 by KVH Industries;
- Magnetometer: HMR3300 by Honeywell;
- GPS receiver: GNSS OEM receiver C1 by bynav;
- Air data system: Pitot-Static System PSS-8 by Simtec AG.

Fig. 1: FTI unit, assembled.

Fig. 2: FTI unit, disassembled.

III. Results

The results presented in this section pertain two separate performance assessments that were carried out regarding the integration between the attitude estimation algorithm and the aerodynamic angle estimator ASSE. Firstly, the attitude estimation algorithm was tested independently from ASSE by means of a series of tests performed using the FTI unit with a single-axis motion table at the National Metrology Institute of Italy (INRiM); these tests were aimed at assessing the estimation accuracy around two axes (pitch and roll). Secondly, the integration between the attitude estimation algorithm and ASSE has been verified by means of flight simulation data.

The values of all the parameters that were used to perform the tests hereby presented are reported in TABLE I.

TABLE I: Values of the parameters for both algorithms

Parameter	Value	Unit
α	10^{-3}	[-]
β	2	[-]
κ	3	[-]
$\sigma_p^2,\sigma_q^2,\sigma_r^2$	$5 \cdot 10^{-7}$	$(rad/s)^2$
$\sigma_u^2,\sigma_v^2,\sigma_w^2$	10^{-4}	$(m/s)^2$
$\sigma_{\dot{u}}^2,\sigma_{\dot{v}}^2,\sigma_{\dot{w}}^2$	10^{-4}	$(m/s^2)^2$
$\sigma_{a_x}^2,\sigma_{a_y}^2,\sigma_{a_z}^2$	$5 \cdot 10^{-5}$	$(m/s^2)^2$
ζ	1	[-]
ω_0	0.4π	[-]

A. INRiM tests

At INRiM, four separate tests were performed to assess the pitch and roll angle estimation capabilities of the presented algorithm based on UKF and CF. The tests were carried out by mounting the FTI unit on a single-axis motion table and commanding a series of rotations around one axis at a time. The measurements of the FTI unit were then retrieved and processed with the algorithm. The four tests are the following:

- *Test # 1*: roll rotations from -10° to 10° with steps of 1°;
- *Test # 2*: roll rotations from -180° to 180° with steps of 20°;
- *Test # 3*: pitch rotations from -90° to 90° with steps of 20°;
- *Test # 4*: pitch rotations from -5° to 5° with steps of 1°.

All tests were performed by commanding the desired angle for around 10 s before commanding the next one. The results are displayed in Fig. 3a–3d. The plots display, for each commanded rotation angle, the estimation error (computed as the difference between the mean estimated value and the commanded one) and the estimation variance.

It is possible to observe that for both roll and pitch angles, the mean estimation error varies along the angle range. In particular, the mean roll estimation error reaches its minimum absolute value at around 0°, whilst the mean pitch estimation error minimum is found at around 5°. Both errors remain in the order of magnitude of 10^{-1} ° and reach their maximum values at the extremities of the range.

B. Integration tests

In order to evaluate the performance of both algorithms when they are integrated, a test was performed by means of

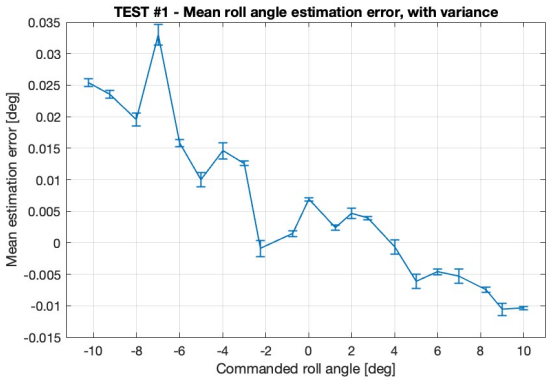

(a) Results of test # 1.

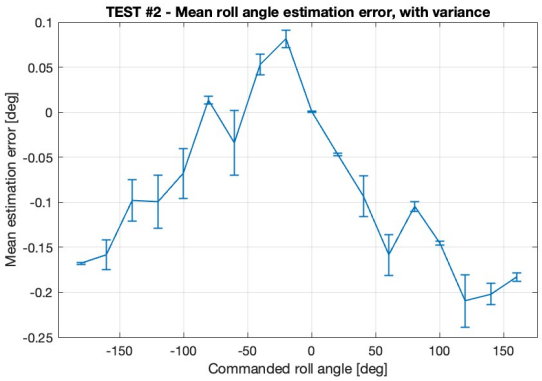

(b) Results of test # 2.

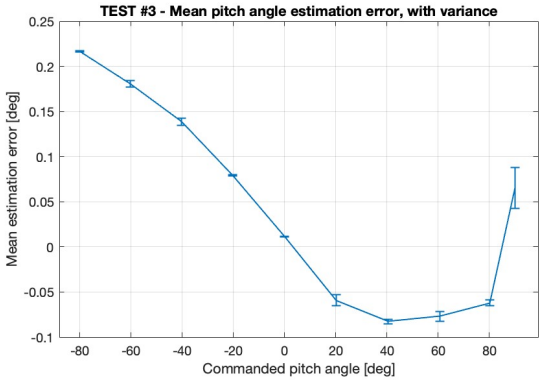

(c) Results of test # 3.

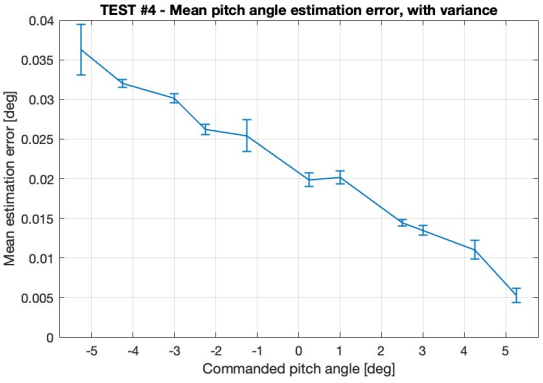

(d) Results of test # 4.

Fig. 3: Test results.

flight simulator data. The flight simulator is a nonlinear six-degree-of-freedom aircraft model with nonlinear aerodynamic and thrust models. The simulation is executed with 10 ms fixed time steps aiming to be coherent with the output rate of the FTI unit. The test was performed in MATLAB.

The results of the test are shown in Fig. 4–6. The flight simulation features a commanded elevator doublet and a commanded rudder doublet, both starting at 10 s and ending at 14 s. It can be seen in Fig. 4 and 5 that the attitude estimation yields a better performance with respect to the one seen in the INRiM tests: this is due to the fact that the latter were performed with real instrumentation, whereas the test hereby considered pertains to a flight simulation.

The ASSE algorithm, on the other hand, manages to estimate the aerodynamic angles with an error in the order of magnitude of 10^{-1} ° for most of the selected time range.

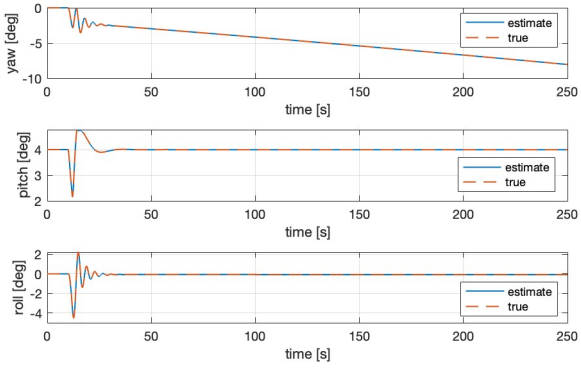

Fig. 4: Integration test - estimated Euler angles versus true values.

IV. Conclusion

This work presents the integration of an attitude estimation algorithm based on a combination of UKF and CF with a synthetic air data sensor for the aerodynamic angles called ASSE. Both algorithms are described in detail. Then, the results of a series of tests aimed at verifying and assessing their performance are presented.

The attitude estimation algorithm is tested independently from ASSE by means of four tests, carried out using a single-axis motion table at INRiM. The data are collected using an FTI unit comprising a MEMS accelerometer, a FOG gyroscope, a GPS receiver, a magnetic compass and a Pitot-static probe. The tests are carried out by commanding a series of rotation angles spanning the whole range for both pitch and roll; each angle is commanded for around 10 s before commanding the next one.

The results show that the algorithm is able to withstand the

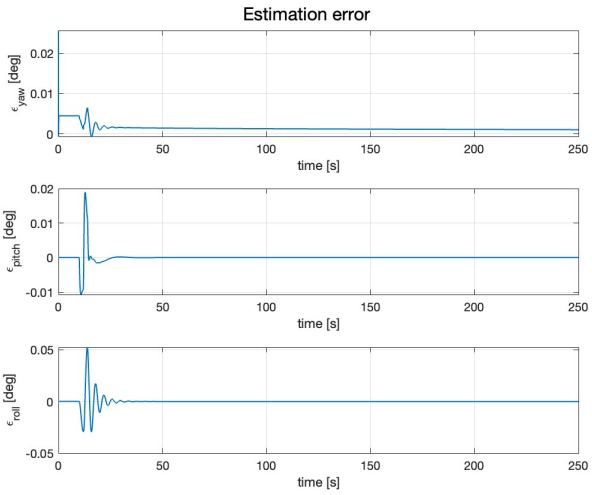

Fig. 5: Integration test - Euler angles estimation error.

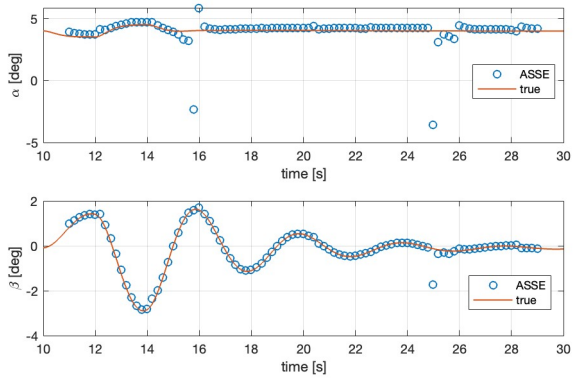

Fig. 6: Integration test - Aerodynamic angles estimation.

sensor noise and provide a maximum estimation error in the order of 10^{-1}°, for both pitch and roll.

Then, the integration between ASSE and the attitude estimation algorithm is assessed by means of flight simulation data obtained with a nonlinear aircraft model. The attitude estimation proves to be more accurate than the one observed during the INRiM tests, as expected. The ASSE algorithm provides an estimation error in the order of 10^{-1}°. The evaluated performance of both algorithms can be deemed satisfactory for the scope of the present work, which paves the way for future developments which include a performance assessment of the integrated algorithms with flight data.

REFERENCES

[1] A. Lerro, A. Brandl and P. Gili, "Model-Free scheme for Angle-of-Attack and Angle-of-Sideslip estimation," Journal of Guidance, Control and Dynamics, vol. 44, no. 3, pp. 595–600, 2021.

[2] Julier, S.J. and Uhlmann, J.K., "A new extension of the Kalman Filter to nonlinear systems", Proceedings Volume 3068, Signal Processing, Sensor Fusion and Target Recognition VI, 1997.

[3] Crassidis, J.L. and Markley, F.L., "Unscented filtering for spacecraft attitude estimation", Journal of Guidance Control and Dynamics, Vol. 26, No. 4, pp. 536–542, 2003.

[4] Shin, E. H. and El-Sheimy, N., "An Unscented Kalman Filter for in-motion alignment of Low-Cost IMUs", Proceedings of the 2004 Position Location and Navigation Symposium, pp. 273–279, 2004.

[5] VanDyke, M. C., Schwartz, J. L. and Hall, C. D., "Unscented Kalman filtering for spacecraft attitude state and parameter estimation", Proceedings of the AAS/AIAA space flight mechanics conference, No. AAS 04-115, 2004.

[6] Zhao, L., Nie, Q. and Guo, Q., "Unscented Kalman filtering for SIS attitude estimation", Proceedings of the 2007 IEEE International Conference on Control and Automation, pp 228–232, 2007.

[7] Wan, E.A., van der Merwe, R., "The Unscented Kalman filter for nonlinear estimation", Proceedings of the IEEE 2000 Adaptive Systems for Signal Processing, Communications, and Control Symposium, 2000.

[8] J.K. Shiau e I.C. Wang, "Unscented Kalman Filtering for Attitude Determination Using MEMS Sensors," Journal of Applied Science and Engineering, Vol. 16, No. 2, pp. 165–176, 2013.

[9] A. Lerro, "Physics-based modelling for a closed form solution for flow angle estimation," Advances in Aircraft and Spacecraft Science, Vol. 8, No. 4, pp. 273–287, 2021.

[10] A. Lerro, "Survey of Certifiable Air Data Systems for Urban Air Mobility," 2020 AIAA/IEEE 39th Digital Avionics Systems Conference (DASC), San Antonio, TX, USA, 2020, pp. 1–10.